pH-degradable mannosylated nanogels for dendritic cell targeting

Ruben De Coen,[a] Nane Vanparijs,[a] Martijn D. P. Risseeuw,[a] Lien Lybaert,[a] Benoit Louage,[a] Stefaan De Koker,[b] Vimal Kumar,[b] Johan Grooten,[b] Leeanne Taylor,[c] Neil Ayres,[c] Serge Van Calenbergh,[a] Lutz Nuhn,[a] Bruno G. De Geest[a*]*

[a] Department of Pharmaceutics, Ghent University, Ghent, Belgium.

[b] Department of Biomedical Molecular Biology, Ghent University, Ghent, Belgium.

[c] Department of Chemistry, University of Cincinnati (OH), US.

KEYWORDS

Nanogels, dendritic cells, mannose, block copolymers, self-assembly

ABSTRACT

We report on the design of glycosylated nanogels via core-cross-linking of amphiphilic non- water-soluble block copolymers composed of an acetylated glycosylated block and a pentafluorophenyl (PFP) activated ester block prepared by RAFT polymerization. Self-assembly, pH-sensitive core-cross-linking and removal of remaining PFP esters and protecting groups is achieved in one-pot yielding fully hydrated sub-100 nm nanogels. Using cell subsets that exhibit high and low expression of the mannose receptor under conditions that suppress active endocytosis, we show that mannosylated but not galactosylated nanogels can efficiently target the mannose receptor (MR) that is expressed on the cell surface of primary dendritic cells (DCs). These nanogels hold promise for immunological applications involving DCs and macrophage subsets.

INTRODUCTION

Mannose-binding cell surface receptors are attractive therapeutic and diagnostic targets.[1] The mannose receptor CD206 is a carbohydrate binding protein (i.e. lectin) and an endocytotic receptor expressed on the surface of dendritic cells (DCs), which are the most potent professional antigen presenting cells of the immune system and a primary target cell population for vaccine delivery and immuno-therapy.[2] In this regard, mannosylation using recombinant or enzymatic routes of protein vaccine antigens has shown to be a promising strategy to enhance the adaptive immune response.[3] Mannose receptors are also expressed on a macrophage subset that is found in solid tumors, termed tumor associated macrophages (TAMs) that exert a pro-tumoral function and thus are a target for eradication or reprogramming.[4] Moreover, the C-type lectin DC-SIGN (also termed CD209)[5] that is expressed on the surface of DCs and macrophages recognizes mannose residues

expressed on the surface of the HIV virus, which is the first hallmark of the cellular entry of this virus. Competing for entry of the virus or delivering an anti-viral compound to infected cells both have therapeutic value in this case. [6,7]

Consequently, there is a clear rationale for the development of engineered nanocarriers that can target mannose-binding receptors with a therapeutic or diagnostic payload. However, carbohydrate-lectin recognition is a classic example of low affinity binding that can take strong profit from presenting multiple copies of the same ligand onto a nanoparticle surface to enhance cell binding and/or internalization.[8] This phenomenon is often referred to as the cluster glycoside effect[9], where clustering of carbohydrates leads to high avidity receptor binding. Indeed, exploiting multivalency[10,11] for targeting nanoparticles to cell surface receptors is an often explored route in diagnostics and drug delivery. Whereas recombinant and enzymatic glycobioengineering routes are well suited for the design of à la carte glycosylated proteins, they are less suited for the design of fully synthetic higher order structures. By contrast, the latter can be obtained through the use of so-called synthetic glycopolymers that exist of monomeric carbohydrate-bearing repeating units.[12,13]

With regard to immuno-therapy, there is a strong rationale for delivering vaccine antigens and immune-stimulatory cues to DCs in nanoparticulate form.[14–16] Relative to soluble antigens, antigens formulated as nanoparticles promote cross-presentation to $CD8^+$ T-cells that can differentiate into cytotoxic T-cells that can recognize and eliminate infected and malignant cells.[16–22] Furthermore, ligating immune-stimulatory small molecules to supramolecular structures should reduce systemic levels and confine the inflammatory activity to lymphatic tissues.[23,24]

Although, the synthesis of mannosylated polymers and nanoparticle derived thereof has been extensively reported[7,25–27] and explored for DC targeting[28,29], the efficacy of unambiguously targeting the mannose receptor CD206 on DCs remains elusive. This can be attributed to the use of

immortalized DC cell lines[30] that only show low expression of the mannose receptor or the use of controls that could exhibit inherent fewer cell interaction. For example, using well known stealth polymer based systems such as poly(ethylene glycol)[29] might yield false negatives due to inherent decreased physicochemical rather than biochemical interaction between polymer and living cells.

Here we report on the fabrication of mannosylated hydrogel nanoparticles (i.e. nanogels) with degradability in a relevant pH-window for endosomal disassembly.[31] To demonstrate the receptor-specific binding to cells expressing the mannose receptor, we first elucidated the expression levels of the mannose receptor on two types of DCs. Second, we also prepared galactosylated nanogels, that in contrast to often used poly(ethylene glycol)-based controls[29] or non-functionalized controls, are expected to witness similar non-specific interactions with the cell membrane as mannose-based nanogels, but are not expected to exhibit ligand-receptor based biochemical interaction. To design nanocarriers for DC-specific targeting, we elaborated on an elegant assembly approach starting from well-defined precursor block copolymers of which both blocks are hydrophobic, but one block is soluble in DMSO and the other not. The latter is based on pentafluorophenyl (PFP) activated ester repeating units. This property allows controlled self-assembly into micellar nanostructures followed by cross-linking and fluorescent labeling under anhydrous conditions, thereby avoiding the competition with hydrolysis of the activated esters that should occur in aqueous medium. Final conversion of remaining PFP-esters into hydrophilic units and deprotection of the other polymer block followed by transfer to the aqueous phase yields fully hydrated nanogels with sub 100 nm dimensions that can be tailored based on the block copolymer length. Importantly, further attributing to the attractiveness of our approach, the full assembly process can be done in a one-pot assembly strategy which favors controllability and reproducibility over the system.

EXPERIMENTAL PROCEDURES

Materials

Unless otherwise stated, all chemicals were purchased from Sigma Aldrich. 2, 2'-azobis(2-methylpropionitrile) (AIBN) was provided by Wako Chemicals and purified by recrystallization from diethyl ether prior to use. The RAFT agent 2-(butylthiocarbonothioylthio)propanoic acid (PABTC) was synthesized according to literature.[32] Silver trifluoromethanesulfonate was purchased from Acros Organics. 1, 2, 3, 4, 6-penta-*O*-acetyl-α-D-mannose, 2, 3, 4, 6-tetra-*O*-acetyl-α-D-galactose bromide, D-mannose and D-galactose were obtained from Carbosynth. 5, 5'-dithio-bis-(2-nitrobenzoic acid) (Ellman's reagent) was provided by G-Biosciences. Female C57BL/6 mice were purchased from Janvier and housed in a specified pathogen-free facility in microisolator units. Cell culture medium and supplements, DPBS (+ $CaCl_2$; + $MnCl_2$), 5-(and 6-)-((N-(5-aminopentyl)amino)carbonyl)tetramethyl rhodamine, Hoechst and Cholera Toxin Subunit B-Alexa Fluor® 488 Conjugate (CTB-AF488) were purchased from Life Technologies. Fc block, MHCII-AF488, CD11c-PE, CD86-PECy7 and CD206-AF647 were obtained from BD Pharmingen.

Instrumentation

All ^{1}H-, ^{13}C-, and ^{19}F-NMR spectra were recorded on a Bruker 300 MHz FT-NMR spectrometer. Chemical shifts (δ) were provided in ppm relative to TMS. Samples were prepared in chloroform-d, DMSO-d_6 and deuterated water and their signals referenced to residual non-deuterated signals of the solvent. Molecular weight determination was obtained using size exclusion chromatography (SEC) in tetrahydrofuran (THF) as solvent. This system consisted of a PU 1580 pump, AS 1555 auto sampler, UV 1575 UV-detector (detection at 254 nm), RI 1530 RI-detector from JASCO. Columns were purchased at MZ-Analysentechnik: MZ-Gel SDplus 102 Å and MZ-Gel SDplus

106 Å. Calibration was done using polystyrene standards purchased from Polymer Standard Services. ESI-mass spectroscopy was performed on a Waters LCT Premier XE TOF equipped with an electrospray ionization interface and coupled to a Waters Alliance HPLC system.

Synthesis of pentafluorophenyl acrylate (PFPA)

Pentafluorophenyl acrylate was synthesized according to literature.[33] Pentafluorophenol (33.31 g, 181 mmol) was dissolved in 150 mL anhydrous dichloromethane (DCM) under inert atmosphere at 0 °C. Triethylamine (26.75 mL, 190 mmol) was pre-dried using sodium sulfate and added dropwise to the cooled reaction mixture. Acryloyl chloride (15.6 mL, 186.4 mmol) was added dropwise to the solution under vigorous stirring and after 30 min, the reaction was allowed to reach room temperature and stir for an additional 2 h. Monitoring of the reaction was performed by thin-layer chromatography (TLC; Hexane:EtOAc 80:20; R_f = 0.70) until complete consumption of pentafluorophenol was observed. The reaction mixture was filtered prior to twofold extraction with brine and dried over sodium sulfate before concentrating the organic phase under vacuum. The crude product (brown oil) was purified by vacuum distillation after the addition of 10 mg mono methyl ether hydroquinone (MEHQ to inhibit autopolymerization) and yielded a clear oil (40.8 g, 95 % yield). ^{19}F-NMR (282 MHz, $CDCl_3$, **Figure S1**): δ (ppm): -152.7 (d; J = 16.9 Hz; 2F; o-C_6F_5); -158.1 (t; J = 21.6 Hz; 1F; p-C_6F_5); -162.5 (t; J = 19.2 Hz; 2F; m-C_6F_5). ^{1}H-NMR (300 Mz, $CDCl_3$, **Figure S2**), δ (ppm): 6.72 (dd; J = 17.2, 1.1 Hz, 1H; -CH=**CH_2**); 6.37 (dd; J = 17.2, 10.5 Hz; 1H; -**CH**=CH_2); 6.17 (dd; J = 10.5, 1.1 Hz; 1H; -CH=**CH_2**)

Synthesis of 2, 3, 4, 6-Tetra-*O*-Acetyl-α-D-Mannosylethyl Acrylamide (TAManEAm)

1, 2, 3, 4, 6-penta-*O*-acetyl-α-D-mannose (11.71 g, 30 mmol) was dissolved in DCM (125 mL) prior to the dropwise addition of *N*-hydroxyethyl acrylamide (7.12 g, 60 mmol) under inert N_2

atmosphere. The solution was placed in an ice bath and 27.8 mL (225 mmol) boron trifluoride diethyl etherate was added dropwise over 45 min. The mixture was kept in an ice bath for 1 h before the reaction was allowed to reach room temperature. Monitoring via TLC (Hexane:EtOAc 20:80, R_f = 0.20) indicated complete consumption of 1, 2, 3, 4, 6-penta-*O*-acetyl-α-D-mannose after 36 h of reaction. The mixture was poured into ice water and extracted twice. The aqueous layer was extracted once with DCM and the organic layers were combined, washed (2 times with saturated sodium bicarbonate solution, 1 time with brine), dried over sodium sulfate and concentrated under vacuum. The resulting crude product (pale yellow oil) was purified by silica gel column chromatography (Hexane:EtOAc 20:80) and yielded a pale yellowish gum after concentration under vacuum (86.8 % yield). ^{1}H-NMR (300 MHz, $CDCl_3$, **Figure S3**), δ (ppm): 6.34 (t; J = 4.9 Hz; 1H; -CO-**NH**-); 6.27 (ddd; J = 17.0, 5.6, 1.7 Hz; 1H; -CH=**CH_2**); 6.12 (ddd; J = 16.9, 14.5, 9.9 Hz; 1H; -**CH**=CH_2); 5.62 (ddd; J = 10.1, 3.9, 1.7 Hz; 1H; -CH=**CH_2**); 5.31 – 5.16 (m; 3H; -**CH**-(OAc)-); 4.78 (d; J = 1.6 Hz; 1H; **α-CH**); 4.26 – 4.02 (m; 2H; -**CH_2**-OAc); 3.94 (ddd; J = 9.6, 5.6, 2.5 Hz; 1H; -C**H**-CH2-OAc); 3.79 (ddd; J = 9.5, 6.8, 3.4 Hz; 1H; -O-C**H**H-CH2-NH-); 3.65 - 3.41 (m; 3H; -O-CH**H**-C**H_2**-NH-); 2.11 (s; 3H; -**OAc**); 2.05 (s; 3H; -**OAc**); 2.01 (s; 3H; -O**Ac**); 1.96 (s; 3H; -**OAc**). APT ^{13}C-NMR (75 MHz, $CDCl_3$, **Figure S4**), δ (ppm): 170.50 (-O-**CO**-CH_3); 169.9 (2 x -O-**CO**-CH_3); 169.57 (-O-**CO**-CH_3); 165.85 (-NH-**CO**-CH-CH_2); 130.5 (-NH-CO-**CH**-CH_2); 126.7 (-NH-CO-CH-**CH_2**); 97.63 (-α-**CH**-); 69.23 (-CH_2-CH-**CH**(OAc)-); 68.91 (-CH_2-**CH**-CH(OAc)-); 68.62 (-CH_2-CH-CH-**CH**(OAc)-); 67.37 (-CO-NH-CH_2-**CH_2**-); 66.01 (-α-CH-**CH**(OAc)-); 62.37 (-CH-**CH_2**-OAc); 39.00 (-CO-NH-**CH_2**-CH_2-); 20.73 (-O-CO-**CH_3**); 20.60 (O-CO-**CH_3**); 20.58 (2 x O-CO-**CH_3**).

MS (ESI): calculated for $C_{19}H_{27}NO_{11}H$ $[M+H]^+$, 446.1657; found 446.1671; $C_{19}H_{27}NO_{11}Na$ $[M+Na]^+$, 468.1476; found 468.1482; $C_{19}H_{27}NO_{11}K$ $[M+K]^+$, 484.1216; found 484.1481.

Synthesis of 2, 3, 4, 6-Tetra-*O*-Acetyl-β-D-Galactosylethyl Acrylamide (TAGalEAm)

2, 3, 4, 6-tetra-*O*-acetyl-β-D-galactosylethyl acrylamide is synthesized by utilizing the Koenigs-Knorr reaction according to literature.[34] 2, 3, 4, 6-tetra-*O*-acetyl-α-D-galactopyranosyl bromide (2.224 g, 20 mmol) was dissolved in a round bottom flask containing anhydrous DCM (200 mL) and 20 g of 4 Å molecular sieves. The correct amount of *N*-hydroxyethyl acrylamide (7.12 g, 60 mmol) was added dropwise under inert N_2 atmosphere. The solution was cooled down to -20 °C and purged with nitrogen under vigorous stirring for 1 h. The round bottom flask was covered in aluminum foil in order to protect the reaction from light. Afterwards, 6.17 g (1.2 eq, 24 mmol) of silver trifluoromethanesulfonate was added to the reaction mixture and left to react for 24 h in an ice bath in the absence of light. **Figure S7** illustrates the chemical reaction. Monitoring via TLC (Hexane:EtOAc 30:70, $R_f = 0.25$) indicated the complete consumption of 2, 3, 4, 6-tetra-*O*-acetyl-α-D-galactopyranosyl bromide after 24 h of reaction. The reaction mixture was filtered over Celite®545, poured into saturated sodium bicarbonate solution and extracted twice. The aqueous layer was extracted once with DCM and the organic layers were combined, washed with brine, dried over sodium sulfate and concentrated under vacuum. The resulting crude product (pale yellow oil) was purified by silica gel column chromatography (Hexane:EtOAc 30:70) and yielded a pale yellowish gum after concentration under vacuum (56 % yield). ^{1}H-NMR (300 MHz, $CDCl_3$, **Figure S8**), δ (ppm): 6.30 (ddd; J = 17, 1.3 Hz; 1H; -CH=**CH_2**); 6.10 (ddd and br; J = 17.0, 10.2, 2.9 Hz; 2H; -CH=**CH_2** and -CO-**NH**-); 5.67 (ddd; J = 10.2, 2.5, 1.5 Hz; 1H; -**CH**=CH_2); 5.41 (dd; J = 3.4, 1.2 Hz; 1H; -**CH**-(OAc)-); 5.19 (dd; J = 10.5, 7.8 Hz; 1H; -**CH**-(OAc)-); 5.02 (dd; J = 10.5, 3.4 Hz; 1H; -**CH**-(OAc)-); 4.47 (d; J = 7.8 Hz; 1H; **β-CH**); 4.20 - 4.10 (m; 2H; -**CH_2**-OAc); 3.97 – 3.86 (m; 2H; -**CH**-CH2-OAc; -O-**CH**H-CH2-NH-); 3.74 (ddd; J = 10.2, 7.2, 3.4 Hz; 1H; -O-CH**H**-CH2-NH-); 3.70 - 3.43 (m; 2H; -O-CHH-**CH_2**-NH-); 2.16 (s; 3H; -O**Ac**); 2.05 (s; 3H; -

O**Ac**); 2.05 (s; 3H; -O**Ac**); 1.99 (s; 3H; -O**Ac**). APT ^{13}C-NMR (75 MHz, $CDCl_3$, **Figure S9**), δ (ppm): 170.79 (-O-**CO**-CH_3); 170.55 (-O-**CO**-CH_3); 170.45 (-O-**CO**-CH_3); 170.16 (-O-**CO**-CH_3); 165.82 (-NH-**CO**-CH-CH_2); 131.09 (-NH-CO-**CH**-CH_2); 127.08 (-NH-CO-CH-**CH_2**); 101.87 (-β-**CH**-); 71.27 (-CH_2-CH-**CH**(OAc)-); 71.07 (-CH_2-**CH**(OAc)-); 69.53 (-CO-NH-CH_2-**CH_2**-); 69.35 (-CH_2-CH-CH-**CH**(OAc)-); 67.36 (-β-CH-**CH**(OAc)-); 61.78 (-CH-**CH_2**-OAc); 39.55 (-CO-NH-**CH_2**-CH_2-); 21.25 (-O-CO-**CH_3**); 21.07 (O-CO-**CH_3**); 21.06 (O-CO-**CH_3**); 20.96 (O-CO-**CH_3**).

MS (ESI): calculated for $C_{19}H_{27}NO_{11}H$ $[M+H]^+$, 446.1657; found 446.1657; $C_{19}H_{27}NO_{11}Na$ $[M+Na]^+$, 468.1476; found 468.1471; $C_{19}H_{27}NO_{11}K$ $[M+K]^+$, 484.1216; found 484.1217.

Synthesis of poly(2, 3, 4, 6-Tetra-*O*-Acetyl-α-D-Mannosylethyl Acrylamide)$_x$ (*p*(TAManE-Am$_x$))

For a typical polymerization reaction with a theoretical degree of polymerization (DP) of 100, 4.0 g TAManEAm (9 mmol), 21.4 mg PABTC CTA (0.09 mmol), 2.96 mg AIBN (148.0 µL of a 0.02 mg/µL stock solution, 0.018 mmol) where dissolved in 8.852 mL 1, 4-dioxane to obtain a final monomer concentration of 1M. The solution was transferred to a Schlenk vial and degassed by 5 subsequent freeze-pump-thaw cycles before being back filled with nitrogen. The Schlenk vial was placed inside a pre-heated oil bath of 80 °C. After 45 minutes, the polymerization was quenched by cooling the vial in ice water and exposing the reaction to oxygen. Conversion was calculated by ^{1}H-NMR spectra of the reaction mixture in $CDCl_3$. The reaction mixture was purified by triple precipitation into ice-cold diethyl ether and dried for 24 h in a vacuum oven at 40 °C. The resulting pure polymer was used as macro CTA for the synthesis of the desired block copolymers. The macro CTA was analyzed using THF-SEC to determine the M_n, M_w and Đ. The theoretical M_n was calculated based on the conversion determined by ^{1}H-NMR (**Table S1**).

Synthesis of *p*(Tetra-*O*-Acetyl-α-D-Mannosylethyl Acrylamide$_x$-b-PFPA$_y$) (*p*(TAManEAm$_x$-b-PFPA$_y$))

For a block copolymer polymerization with a theoretical DP of 216, 471 mg PFPA (2 mmol), 298 mg *p*(TAManEAm$_{72}$) macro CTA (0.0093 mmol), 0.304 mg AIBN (15.20 µL of a 0.02 mg/µL stock solution, 0.00185 mmol) where dissolved in 2.485 mL 1, 4-dioxane to obtain a final monomer concentration of 0.8M. The solution was transferred to a Schlenk vial and degassed by 5 subsequent freeze-pump-thaw cycles before being back filled with nitrogen. The Schlenk vial was placed inside a pre-heated oil bath of 80 °C. After 21 h, the polymerization was quenched by cooling the vial in ice water and exposing the reaction to oxygen. Conversion was calculated by ^{19}F-NMR spectra of the reaction mixture in $CDCl_3$. The reaction mixture was purified by triple precipitation into ice-cold hexane and dried for 24 h in a vacuum oven at 40 °C. The resulting pure block copolymer was analyzed using THF-SEC to determine the M_n, M_w and Đ (**Figure S12**). The theoretical M_n was calculated based on the conversion determined by ^{19}F-NMR (**Table S1**). Although **Table S1** shows desirable conversion of the PFPA monomer, no shift in SEC traces is obtained (**Figure S12**). A possible explanation for this anomaly is the formation of a radically polymerized *p*PFPA homopolymer instead of RAFT chain extension to the already existing acetylated mannose-bearing polymer. This hypothesis is in line with the increase of Đ and the lack of shift in the GPC trace. These polymers did not fully dissolve in DMSO and were not further analyzed by DLS, nor used in further experiments.

Synthesis of poly(Pentafluorophenyl Acrylate) (*p*(PFPA$_x$))

A detailed example of a reaction with a theoretical degree of polymerization (DP) of 250 is described below; further polymerization reactions with lower DP's (respectively DP 100 and DP 50) were performed analogously to the provided protocol. For a typical polymerization reaction, 1.9 g PFPA (8 mmol), 7.62 mg PABTC CTA (152 µL of a 0.05 mg/µL stock solution, 0.032 mmol), 1.05 mg AIBN (52.5 µL of a 0.02 mg/µL stock solution, 0.0064 mmol) where dissolved in 7.795 mL 1, 4-dioxane, to obtain a final monomer concentration of 1M. The solution was transferred to a Schlenk vial and degassed by 5 subsequent freeze-pump-thaw cycles before being back filled with nitrogen. The Schlenk vial was placed inside a pre-heated oil bath of 80 °C. After 3 h, the polymerization was quenched by cooling the vial in ice water and exposing the reaction to oxygen. Conversion was calculated by ^{19}F-NMR spectra of the reaction mixture in $CDCl_3$. The reaction mixture was purified by triple precipitation into ice-cold hexane and dried for 24 h in a vacuum oven at 40 °C. The resulting purified polymer was used as macro CTA for the synthesis of the desired block copolymers. The macro CTA was analyzed using THF- SEC to determine the M_n, M_w and Đ. The theoretical M_n was calculated based on the conversion determined by ^{19}F-NMR. **Figure S13** illustrates the ^{19}F-NMR spectrum of a purified *p*(PFPA$_x$) macro CTA, exemplified for P 3. ^{19}F-NMR (282 MHz, $CDCl_3$, **Figure S13**): δ (ppm): -153.22 (br, 2F; o-C_6F_5); -156.79 (br, 1F; p-C_6F_5); -162.26 (br, 2F; m-C_6F_5).

Synthesis of p(PFPA$_x$-b-Tetra-O-Acetyl-α-D-Mannosylethyl Acrylamide$_y$) (p(PFPA$_x$-b-TA-ManEAm$_y$))

A detailed example of a chain extension reaction with a theoretical degree of polymerization (DP) of 167 is stated below. Reactions with lower DP's (respectively DP 80 and DP 40) were performed

analogously to the provided protocol. For a typical block copolymerization reaction, 891 mg tetra-*O*-acetyl-α-D-mannosylethyl acrylamide (2 mmol), 450 mg *p*(PFPA)$_{157}$ macro CTA (0.012 mmol), 0.394 mg AIBN (19.7 µL of a 0.02 mg/µL stock solution, 0.0024 mmol) and 2.48 mL 1, 4-dioxane were added to a Schlenk vial and degassed by 5 subsequent freeze-pump-thaw cycles before being back filled with nitrogen. The Schlenk vial was placed inside a pre-heated oil bath of 80 °C. After 45 minutes, the reaction was quenched by cooling the vial in ice water and exposing the reaction to oxygen. Conversion was calculated by ^{1}H-NMR spectra of the reaction mixture in $CDCl_3$ (illustrated by **Figure S14**). Purification of the reaction mixture was performed by triple precipitation into ice-cold diethyl ether. The purified block copolymer was dried under vacuum at 40 °C for 24 h, followed by analysis using a THF-SEC to determine the M_n, M_w and Đ. The theoretical M_n was calculated based on the conversion determined by ^{1}H-NMR (**Table 1**). **Figure S15** illustrates the ^{1}H-NMR spectrum of all purified p(PFPA$_x$-b-TAManEAm$_y$) block copolymers. ^{1}H-NMR (300 MHz, $CDCl_3$, **Figure S15**, exemplified for (1)): δ (ppm): 7.5 – 6.5 (1H; -CO-**NH**-); 5.26 (3H; -**CH**-(OAc)-); 4.90 (1H; **α-CH**); 4.28 (1H; -C**H**-CH2-OAc); 4.07 (2H; -**CH$_2$**-OAc); 3.75 (1H; -O-C**H**H-CH2-NH-); 3.60 – 3.20 (3H; -O-CH**H**-C**H$_2$**-NH-); 3.08 (1H; -CH$_2$-**CH**-CO-O-C$_6$F$_5$); 2.45 (1H; -CH$_2$-**CH**-CO-NH-); 2.25 – 1.5 (br; 16H; 4 x –**OAc**, -**CH$_2$**-CH-CO-O-C$_6$F$_5$, -**CH$_2$**-CH-CO-NH-). ^{19}F-NMR (282 MHz, $CDCl_3$): δ (ppm): -153.22 (br, 2F; o-C$_6$F$_5$); -156.79 (br, 1F; p-C$_6$F$_5$); -162.26 (br, 2F; m-C$_6$F$_5$).

Synthesis of *p*(PFPA$_x$-b-Tetra-*O*-Acetyl-β-D-Galactosylethyl Acrylamide$_y$) (*p*(PFPA$_x$-b-TA-GalEAm$_y$))

For a typical block copolymerization reaction with a theoretical degree of polymerization (DP) of 80, 410 mg tetra-*O*-acetyl-β-D-galactosylethyl acrylamide (0.92 mmol), 181 mg p(PFPA$_{65}$) macro CTA (0.0115 mmol), 0.377 mg AIBN (20 µL of a 0.02 mg/µL stock solution, 0.0023 mmol) and

1.4 mL 1, 4-dioxane were added to a Schlenk vial and degassed by 5 subsequent freeze-pump-thaw cycles before being back filled with nitrogen. The Schlenk vial was placed inside a pre-heated oil bath of 80 °C. After 3 h, the reaction was quenched by cooling the vial in ice water and exposing the reaction to oxygen. Conversion was calculated by ^{1}H-NMR spectra of the reaction mixture in $CDCl_3$. Purification of the reaction mixture was performed by triple precipitation into ice-cold diethyl ether. The purified block copolymer was dried under vacuum at 40 °C for 24 h, followed by analysis using a THF-SEC to determine the M_n, M_w and Đ. The theoretical M_n was calculated based on the conversion determined by ^{1}H-NMR (**Table 1**). **Figure S16** illustrates the ^{1}H-NMR spectrum of the purified block copolymer. ^{1}H-NMR (300 MHz, $CDCl_3$, **Figure S16**): δ (ppm): 7.8 – 6.8 (1H; -CO-**NH**-); 5.40 (1H; -**CH**-(OAc)-); 5.10 (2H; 2 x -**CH**-(OAc)-); 4.61 (1H; **β-CH**); 4.15 (4H; -C**H**-C**H2**-OAc, -O-C**H**H-CH2-NH-); 3.88 (1H; -O-C**H**H-CH2-NH-); 3.44 (2H; -O-CHH-C**H_2**-NH-); 3.08 (br; 1H; -CH_2-**CH**-CO-O-C_6F_5); 2.46 (1H; -CH_2-**CH**-CO-NH-); 2.25 – 1.5 (br; 16H; 4 x –**OAc**, -**CH_2**-CH-CO-O-C_6F_5, -**CH_2**-CH-CO-NH-). ^{19}F-NMR (282 MHz, $CDCl_3$): δ (ppm): -153.22 (br, 2F; o-C_6F_5); -156.79 (br, 1F; p-C_6F_5); -162.26 (br, 2F; m-C_6F_5).

Nanohydrogel synthesis

A detailed example of a one-pot nanohydrogel synthesis for block copolymer 1 (Man_1) is provided below. Analogous reaction conditions were employed for the synthesis of nanogels Man_2 and Man_3 (D and ND). *p*($PFPA_{157}$-b-$TAManEAm_{145}$) block copolymer Man_1 (40.0 mg, 0.39 μmol polymer or 61.4 μmol reactive ester) was transferred into a round-bottom flask equipped with a stirring bar and dissolved in anhydrous DMSO (4.0 mL) under inert atmosphere. The solution was sonicated for 1 h and a 100 μL sample was taken to confirm the formation of self-assembled micellar nano-particles. Fluorescent labeling was performed by adding 16.0 μL 5/6-((N-(5-ami-nopentyl)amino)carbonyl) tetramethyl rhodamine (10 mg/mL stock solution in DMSO, 0.307

μmol) and 5.0 μL of dry triethylamine (35.9 μmol). The reaction was stirred vigorously at room temperature for 24 h before transferring 2.0 mL to another round-bottom flask and putting both in a preheated oil bath of 40 °C. Anhydrous triethylamine (12.8 μL, 92.0 μmol) was added to each reaction vessel together with the desired cross-linker (1.47 μL 2, 2'-bis(aminoethoxy)propane, D, **Figure S17A**; 1.35 μL 2, 2'-(ethylenedioxy)bis(ethylamine), ND, **Figure S17B**; 9.2 μmol) to target 60% cross-linking (i.e. coupling of PFPA repeating units) for each reaction. A 100 μL sample was taken before and after the addition of cross-linker, diluted with $CHCl_3$ and checked using DLS to see the effect of the cross-linker (**Figure S18**). After 24 h of reaction, the remaining PFPA repeating units were removed by the addition of an excess of 2-aminoethanol (9.3 μL, 154 μmol) together with dry triethylamine (64.2 μL, 461 μmol). After an additional 24 h of vigorous stirring, end-capping of the free thiols (residing from the cleaved CTA Z-end group) was performed by addition of 115 μL TCEP in DMSO (50 mg/mL solution) in combination with 530 μL of a 0.1 g/mL *N*-hydroxyethyl acrylamide solution in DMSO. The reaction was cooled down to room temperature after 3 h under continuous stirring. In order to deprotect the acetylated mannose block, 8 mL of dry methanol was added to each reaction mixture. Sodium methoxide (200 μL, 5.4 M concentrated solution in MeOH) was added dropwise and the resulting turbid mixture was kept stirring during 2 h. In order to remove any small byproducts as well as solvents, both reaction mixtures were purified by dialysis against 0.1% v/v ammonium hydroxide solution in demineralized water (with frequent exchange of dialysis medium). After several days, the clear pink solution was lyophilized yielding a fluffy pink powder. To confirm successful deacetylation of the carbohydrate moieties, a ^{1}H-NMR spectrum was recorded of non- cross-linked, 2-aminoethanol treated and deacetylated block copolymers in D_2O (**Figure S19**).

DLS of mannose decorated nanogels

Dynamic light scattering (DLS) of the self-assembled nanogels was done using a Zetasizer Nano-S (Malvern) equipped with a He-Ne laser (λ = 633 nm) as incident beam. Typically, 100 µL samples of a 10.0 mg/mL solution of *p*(PFPA$_x$-b-TAManEAM$_y$) in anhydrous DMSO were sonicated for 15 minutes and filtered (0.450 µm) prior to measurement at 25 °C. Cross-linked nanoparticles were measured under identical conditions, without sonication prior to filtration. After deprotection of the mannose-block and lyophilization, both the non-degradable and the acid-cleavable nanogels were redispersed in DPBS at 5.0 mg/mL, sonicated for 30 minutes, filtered and measured at 25 °C. For each sample, 5 individual measurements were taken and data provided as average ± standard deviation.

Hydrolysis of ketal cross-linked nanogels

The degradability of the nanogels was investigated using 10.0 mg/mL solutions of both Man$_1^D$ and Man$_1^{ND}$ in DPBS (pH 7.4) and 0.1 M sodium acetate buffer (pH 5.0). The lyophilized powder was redispersed, sonicated for 2 minutes, filtered and measured at 25 °C. Spectra were recorded at the start, 1 h, 2 h, 3 h, 4 h, 5 h, 6 h, 24 h and 48 h.

Ellman's Assay

To establish the removal of the thiol end groups by thiol-ene type Michael addition, an Ellman's assay was performed according to the manufacturers' protocol. Aminolysis of the trithio carbonyl moiety by quenching and deprotection with 2-aminoethanol of Man$_2$ is shown in **Figure S20A**. The quenched and deprotected Man$_2$ was used as a thiol bearing control sample and compared with an acid-cleavable Man$_2^D$, where free thiols were end-capped by thiol-ene type Michael addition with *N*-hydroxyethyl acrylamide. Therefore, a 10 mM of 5, 5'-dithiobis-(2-nitrobenzoic acid)

(DTNB) solution in DMSO was diluted 100 fold using a 0.1 M TRIS HCl (pH 7.5) buffering solution. 10 mg/mL solutions of Man_2 and Man_2^D in TRIS HCl buffer (200 µL) were added to 3.8 mL of the diluted DTNB solution, allowed to react for 2 minutes before a UV/VIS spectrum was recorded (350 nm – 800 nm) (**Figure S20B**) using a Shimadzu UV-1650PC UV/VIS double beam spectrophotometer.

Lectin binding assay

The ability of the nanohydrogels to bind mannose-binding lectins was investigated using a Concanavalin A (ConA, 104 kDa) agglutination assay. A 5.0 mg/mL solution of Man_1^D (20 µL) was added to a DLS microcuvet and subsequently diluted using a 80 µL phosphate buffering solution (DPBS, pH 7.4) containing $CaCl_2$ and $MgCl_2$ (respectively 0.901 mM and 0.493 mM). DLS measurements were recorded each 30 s. After 5 minutes, 100 µL of a 1.0 mg/mL ConA in DPBS was added to the microcuvet under continuous recording of the DLS data (**Figure 2E**). Analogous to the above described assay, the lectin binding interaction with galactosylated nanogels was investigated under identical reaction conditions. Afterwards, the solution was equally divided over 2 microcuvets (100 µL's each) and pulsed with 20 µL of either a 0.500 g/mL DPBS solution containing D-Mannose or D-Galactose. The mixture was left to react for an additional 15 minutes before pictures were taken (**Figure S21**).

***In vitro* uptake experiment in murine bone marrow derived DCs**

Bone marrow derived dendritic cells were generated utilizing a protocol modified from literature.[35] Bone marrow was flushed from the femurs and tibias of euthanized twelve-to sixteen-week-old C57BL/6 mice. Red blood cells were lysed using ACK lysis buffer and cells were seeded in 24-well titer plates (150 000 cells per well, suspended in 0.500 mL culture medium containing 10 ng

GM-CSF). Bone marrow derived DCs were cultured in RPMI 1640-glutamax, supplemented with 10 % FCS, 1 mM sodium pyruvate, 1 % penicillin/streptomycin, 1 % MEM NEAA and 50 µM β-mercaptoethanol. Cells were incubated at 37 °C in a controlled, sterile environment of 95 % relative humidity and 5 % CO_2. On day 3, 500 µL of fresh culture medium containing 10 ng CM-CSF was added to each well. Day 6 bone marrow derived DCs were pulsed with 10 or 20 µL of a 10 mg/mL solution of all mannosylated and galactosylated nanogels in DPBS (+ $CaCl_2$ and $MgCl_2$). It should be stated that all samples had comparable fluorescent payload, as measured by a Perkin Elmer Victor 2 plate reader (**Figure S22**). All samples were run in triplicate and the experiment was conducted for 1 h at 4 °C and 37 °C. Special attention was given at the samples at 4 °C, as they were put on ice 1 h prior to pulsing in order to bring their temperature down to 4 °C. After one hour of incubation, the cell suspensions were transferred into Eppendorf tubes and centrifuged immediately (10 min, 250 G, 4 °C). The supernatant was aspirated, discarded and the cell pellets were suspended in 50 µL of antibody cocktail solution containing Fc-block (200 x diluted) and anti-MR CD 206-AF647 (100 x diluted). Unpulsed bone marrow derived DCs were treated with single stains (e.g. MHC II – FITC ss, CD11c ss, CD86-PECy7 ss and anti-MR AF647 ss) in order to set the gating and color compensation for flow cytometry analysis. After 30 min incubation on ice, 200 µL DPBS was added to the samples prior to centrifugation (10 min, 250 G, 4 °C). The supernatant was aspired and the cell pellets were suspended in 200 µL of DPBS and kept on ice to prevent cell lysis. FACS was performed using a BD Accuri C6 (BD Biosciences) and data was processed by FlowJo software. **Figure S23** illustrates the applied gating strategy and proves that MR^{hi} cells are exclusively found on CD11c positive cells, and both on $MHCII^{hi}$ and $MHCII^{low}$ DCs and on both $CD86^{hi}$ and $CD86^{low}$ DCs.

Confocal microscopy on murine bone marrow derived DCs

Murine bone marrow derived DCs were plated out on Willco-Dish glass bottom dishes (50 000 cells, suspended in 200 µL of culture medium) and incubated for 1 h. Next, 7 µL of all mannosylated and galactosylated nanogels were added (10 mg/mL, cfr. highest concentration in FACS experiment) and incubated for 1 h at 37 °C. Fixed cells were simultaneously stained with Hoechst and CTB-AF488. Therefore, after 1 h of incubation, cell culture was aspirated and cells were washed with DPBS (+ $CaCl_2$ and $MgCl_2$). Next, 200 µL of 4 % paraformaldehyde was added and allowed to fixate for 30 minutes. A staining solution was prepared by dissolving 10 µL Hoechst (1 mg/mL stock solution in DMSO) and 5 µL of CTB-AF488 (1 mg/mL stock in DPBS) in a DPBS buffering solution containing 1% BSA (2.5 mL). After aspirating and washing, 200 µL of this staining solution was added to the fixed cells and incubated for 30 minutes at room temperature in absence of light. Finally, the samples were washed with DPBS buffering solution containing 1 % BSA. Confocal microscopy was performed on a Leica DMI6000 B inverted microscope equipped with an oil immersion objective (Leica, 63 x, NA 1.40) and attached to an Andor DSD2 confocal scanner. Images were processed using ImageJ software.

RESULTS AND DISCUSSION

To devise correct conditions for evaluating the role of the mannose receptor, *in vitro* differentiated bone marrow (obtained from the femurs and tibia of mice) derived DCs (bmDCs) and the widely used immortalized DC cell line DC2.4, developed at the Rock lab,[36] were immune-stained against CD11c (a universal DC surface marker) and the mannose receptor CD206. As show in **Figure 1**, there are two distinctly separated subsets in the case of bmDCs that exhibit low (or no) and high CD11c expression, respectively. In total, 80% of the cell population exhibited CD11c

expression and could be regarded as 'true DCs'.[37] Within this population again a significant fraction, i.e. 21% of the total population and 26% of the 'true DCs', but not all, showed co-expression of the mannose receptor CD206. Also, all CD206^{hi} cells were CD11c^{hi} and thus 'true DCs'. Notably, we also observed that expression levels of CD206 on bmDCs decreased over longer time of culturing (>1 week) and with repeated medium exchange and re-seeding in cell culture dishes. As both phenomena contributed to increased levels of DC maturation markers (data not shown), it is important for mannose-receptor targeting studies to use *in vitro* culture conditions that favor a large DC subpopulation to be in immature state.[38]

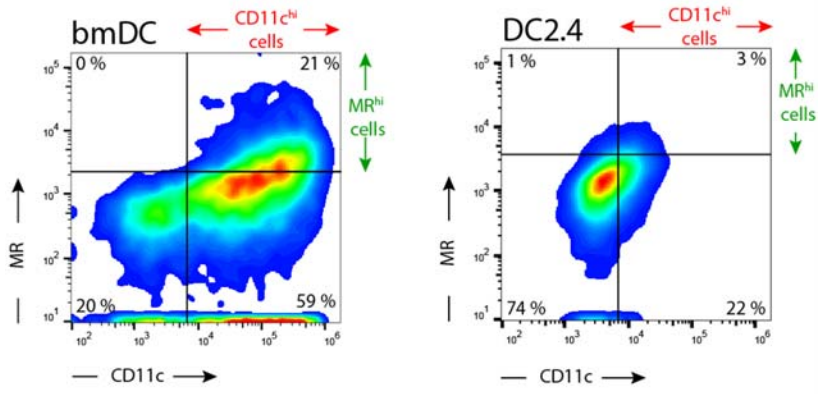

Figure 1. FACS analysis of the expression levels of CD11c and MR by bone marrow derived DCs (at day 5 of the *in vitro* culture) and the immortalized DC2.4 cell line.

By contrast, the immortalized DC2.4 cell line does show expression of both CD11c and CD206, albeit to a much lesser extent than bmDCs. Additionally, no distinct subpopulations could be distinguished, but rather a low and contiguous expression profile was found. Low expression levels of CD206 by DC2.4 have also been confirmed by others.[39] Despite the popularity of the DC2.4 cell line which has extensively been used by many research groups, including our own, for inves-

tigating nanoparticle internalization and antigen presentation, its suitability for investigating mannose-receptor specific targeting is questionable. Moreover, when using bmDCs to investigate the role of the mannose receptor in DC-specific targeting of nanocarriers, we believe it is important, to specifically select the mannose receptor high DC subset in the FACS analysis gating strategy.

Our supramolecular design and one-pot assembly strategy is depicted in **Figure 2**. The key aspect is the ability of block copolymers, comprising a solvophobic poly(pentafluorophenyl acrylate) (*p*PFPA) block to self-assemble in aprotic polar solvents - such as DMSO - into micellar nanoparticles.[33] The activated PFP esters can readily form amide bonds with primary amines in a nearly quantitative way.[40–42] This feature can be exploited to covalently core cross-link these micelles or conjugate bioactives or tracer molecules under non-aqueous conditions, thereby avoiding competition with hydrolysis reactions, that would impair reproducibility. The latter commonly occurs when using the more wide-spread *N*-hydroxysuccinimidyl (NHS) esters in aqueous medium, which are assumed to be less hydrolytically stable than PFP esters.[43] Interestingly, whereas core cross-linked micelles are typically formed using amphiphilic block copolymers containing a hydrophilic and a hydrophobic polymer block, we elaborated onto a strategy that involves two hydrophobic blocks. Our second polymer block is based on poly(tetra-*O*-acetyl-α-D-mannosylethyl acrylamide) block (*p*TAManEAm) that is, contrary to *p*PFPA, well-soluble in DMSO but also non-water soluble. Such approach – i.e. the use of fully hydrophobic precursor polymers for controlled self-assembly of nanostructures that are finally converted into fully hydrated nanostructures – is one of the key synthetic novelties in our work. TAManEAm was synthesized in a convenient one-step reaction by boron trifluoride diethyl etherate catalyzed glycoside formation between peracetylated D-mannose and *N*-hydroxyethyl acrylamide (**Figure 2A**). This route has been elaborated on

for (meth)acrylates[44] but to the best of our knowledge not for (meth)acrylamides that are commonly synthesized via a multistep route based on aminoalkylglycosides.[45,46] The reason that we opt for acrylamides is due to the higher stability of an amide bond, relative to an ester bond (in case of (meth)acrylates)), under conditions, applied further on, that could promote hydrolysis and aminolysis.

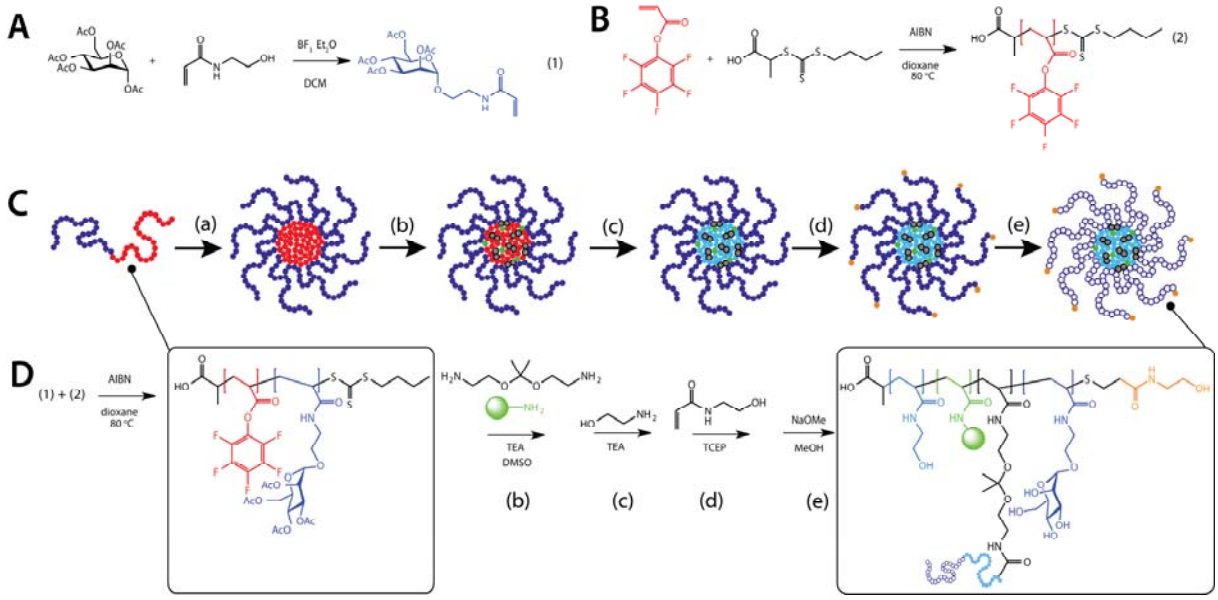

Figure 2. Design and synthesis of mannosylated nanogels. Synthesis of (A) tetra-*O*-acetyl-α-D-mannosylethyl acrylamide and (B) poly(pentafluorophenyl acrylate) macro CTA via RAFT polymerization. (C-D) Schematic overview and corresponding chemical structures of nanogel assembly. (a) Block copolymers self-assemble in DMSO into micellar nanoparticles. (b) Fluorescent labeling and cross-linking (exemplified for the pH-degradable cross-linker 2, 2'-bis(aminoethoxy)propane). (c) Conversion of residual PFP ester with 2-aminoethanol. (d) End-capping of free thiols via Michael-type addition with *N*-hydroxyethyl acrylamide. (e) Deacetylation of the protected mannosyl moieties.

Furthermore, a galactosylated monomer tetra-*O*-acetyl-β-D-galactosylethyl acrylamide (TAGalEAm) was also synthesized that will be used further on (*vide infra*) as a non-MR-binding control polymer. This galactosylated monomer was synthesized using a convenient one-step Koenigs-Knorr reaction (Supporting Information, **Figure S7**).[34] Reversible addition-fragmentation (RAFT)[47] polymerization with 2-(butylthiocarbonothioylthio)propanoic acid (PABTC) as chain transfer agent (CTA) was used to obtain defined block copolymers.

The necessity to use peracetylated monomers arises from the constraints dictated by the use of PFPA as block co-monomer which shows limited solubility in several organic solvents of which none permitted to solubilize deacetylated α-D-mannosylethyl acrylamide (ManEAm) and β-D-galactosylethyl acrylamide (GalEAm). A second constraint that we encountered involves the need to polymerize PFPA prior to chain extension with TAManEAm. The opposite order did not allow for block copolymer formation, which we attribute to the lower reactivity of the acrylamide-based macro CTA relative to its acrylate counterpart[48] (see **Figure S12** for corresponding SEC traces that indicate the formation of two homopolymer populations rather than block copolymers). Four different block copolymers, three mannosylated and one galactosylated (as control), were synthesized with varying chain lengths according to the reaction scheme in **Figure 2D** (synthesis of TAGalEAm is illustrated in **Figure S7**). Size exclusion chromatography (SEC) in THF gave evidence of successful chain extension (**Figure 3A**). Although it could be argued that dispersities are relatively high for RAFT polymerization, this did not affect the self-assembly properties of the block copolymers in DMSO (*vide infra*). Further characterization was done by ^{19}F-NMR and ^{1}H-NMR (**Figures S15**) and **Table 1** summarizes the measured properties of the block copolymers.

Table 1. Polymer composition and properties of the synthesized (block) copolymers and nanogels derived thereof.

#	Composition	DP	T [min]	Con-version [%][a]	M_n[b] [Da]	M_n[c] [Da]	Đ [c]	Size[d] (DMSO) [nm]	PDI (DMSO)	X-link[e]	Size[f] (H_2O) [nm]	PDI (H_2O)
P1	*p*(PFPA$_{157}$)	250	180	63	37600	11700	1.51	-[g]	-[g]	-	-	-
P2	*p*(PFPA$_{65}$)	100	120	65	15700	10800	1.36	-[g]	-[g]	-	-	-
P3	*p*(PFPA$_{33}$)	50	120	67	8200	6900	1.28	-[g]	-[g]	-	-	-
P4	*p*(PFPA$_{65}$)	100	120	65	15700	10800	1.36	-[g]	-[g]	-	-	-
Man$_1$	*p*(PFPA$_{157}$-b-TAManEAM$_{145}$)	167	45	87	102200	23800	1.51	106± 3	0.20	D	106 ± 2	0.19
										ND	93 ± 2	0.14
Man$_2$	*p*(PFPA$_{65}$-b-TAManEAM$_{66}$)	80	45	83	45300	26800	1.37	62 ± 3	0.15	D	41 ± 5	0.25
										ND	41 ± 3	0.16
Man$_3$	*p*(PFPA$_{33}$-b-TAManEAM$_{14}$)	17	45	82	14100	15100	1.19	20 ± 5	0.38	D	22 ± 2	0.39
										ND	19 ± 6	0.38
Gal$_1$	*p*(PFPA$_{65}$-b-TAGalEAM$_{75}$)	80	180	94	49100	28800	1.37	90 ± 4	0.19	-	-	-
										ND	87 ± 3	0.18

a: Determined by 1H-NMR or 19F-NMR (300 MHz or 282 MHz respectively, chloroform-d)

b: Based on the conversion and molecular weight of monomer and CTA

c: Determined by SEC (THF)

d: Z-Average measured by DLS in DMSO

e: Cross-linker: (D) degradable cross-linker 2'-bis(aminoethoxy)propane and (ND) non-degradable cross-linker 2, 2'-(ethylenedioxy)bis(ethylamine)

f: Z-Average measured by DLS in PBS after deprotection of the ManEAm repeating units

g: PFPA MacroCTAs were insoluble in DMSO and were not subjected to further DLS analysis.

All four block copolymers formed self-assembled nanoparticles in DMSO with Z-average sizes of 20, 62 and 106 nm in case of the mannosylated block copolymers and 90 nm for the galactosylated block copolymer, measured by dynamic light scattering (DLS; **Figure 3B** and **Table 1**). These data indicate a good correlation between block copolymer chain length and nanoparticle size.[49,50] Core cross-linking[49] and fluorescent labeling of the self-assembled nanoparticles was performed by addition of a bisamine cross-linker and tetramethylrhodamine cadaverine in presence of triethylamine (**Figure 2D**). Two different cross-linkers (**Figure S17**) were used: the non-degradable

2, 2'-(ethylenedioxy)bis(ethylamine) (abbreviated as ND) and the pH-sensitive 2, 2'-bis(aminoethoxy)propane (abbreviated as D). In case of the galactosylated control nanogel, only the non-degradable cross-linker was used to exclude degradability during experiments. The ketal-containing cross-linker is particularly interesting for biomedical applications[51–53] as it readily degrades in response to the acidic pH that is sensed in endosomes upon cellular endocytosis.[31] Successful cross-linking was evidenced by diluting a sample in chloroform followed by DLS analysis (see supporting information **Figure S18**). Whereas self-assembled precursor block copolymers in DMSO disassemble into unimers upon dilution with chloroform, the cross-linked ones remained invariant, indicating a successful cross-linking strategy. The remaining PFPA repeating units were then reacted with an excess of 2-aminoethanol, thereby transforming the hydrophobic nanoparticle cavity to a hydrophilic environment. Note that at this stage other amine-containing molecules can be installed into the core of the nanoparticles to serve later on for bio-conjugation.

In presence of primary amines, the thiocarbonylthio RAFT Z-end group will be cleaved by aminolysis, leading to nanoparticles with a multitude of free thiols on their surface. We observed that during further work-up nanoparticle aggregation occurred due to disulfide formation, which could be reversed by addition of TCEP or DTT. We do not consider the presence of free thiols on the nanoparticle surface as an issue, but rather as an opportunity. Indeed, Z-end group transformation with divinyl sulfone or methane thiosulfonate has been shown an attractive approach to introduce cysteine-reactive moieties for further bio-conjugation.[41,54–56] Alternatively, the Z-end group can, upon aminolysis, easily be capped by acrylates and acrylamides via Michael addition.[57,58] In the present work we use this route to cap the thiol end-groups by addition of an excess of *N*-hydroxyethyl acrylamide, introducing a hydroxyl group at the polymer chain ends. Near quantitative removal of the thiols was monitored by addition of Ellman´s reagent (**Figure S20**).

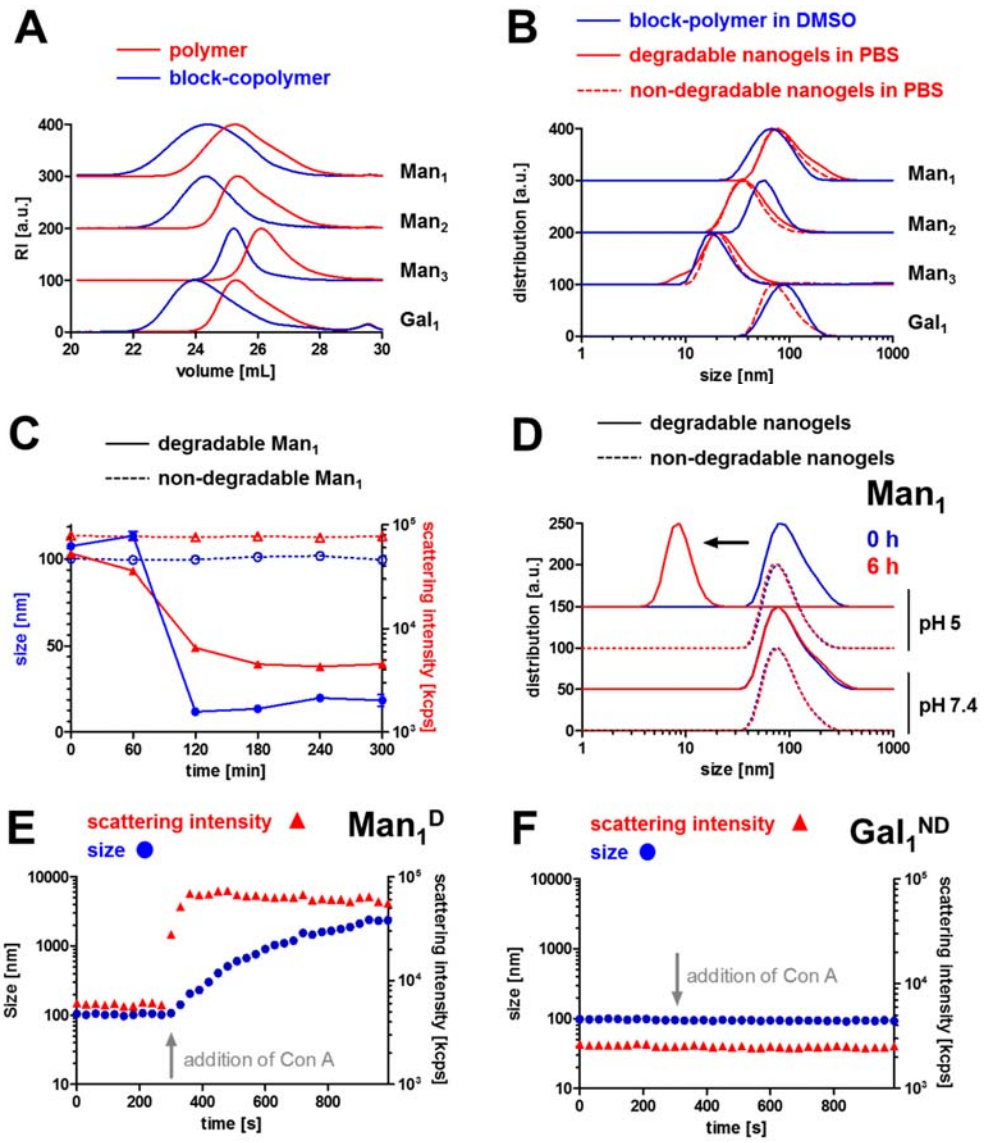

Figure 3. (A) SEC traces in THF of *p*PFPA macro CTA and corresponding *p*(PFPA$_x$-b-TAManEAm$_y$) block copolymers (Man$_1$, Man$_2$, Man$_3$) and *p*(PFPA$_x$-b-TAGalEAm$_y$) block copolymer (Gal$_1$). (B) DLS size distributions of self-assembled nanoparticles (Man$_1$, Man$_2$, Man$_3$ and Gal$_1$) in DMSO and derived nanogels with degradable and non-degradable cross-linkers in PBS. Annotations (Man$_1$), (Man$_2$), (Man$_3$) and (Gal$_1$) correspond to the different polymer compositions listed in Table 1. (C) Evolution of nanogel size and scattering intensity at pH 5 (exemplified for Man$_1^D$ and Man$_1^{ND}$) as function of time at 37°C measured by DLS. (D) Size distribution curves at pH 5 and at pH 7.4 of Man$_1^D$ and Man$_1^{ND}$ after 0 h and 6 h incubation. (E-F) Evolution of size and scattering intensity upon addition of Concanavalin A (ConA) to (E) mannosylated (exemplified for Man$_1^D$) and (F) galactosylated nanogels (Gal$_1^{ND}$) measured by DLS.

In a last reaction step deacetylation was performed by addition of a methanolic sodium methoxide solution (**Figure 2**). Finally, the reaction mixture was extensively dialyzed against a 0.1% (v/v) ammonium hydroxide solution and lyophilized. The ^{1}H-NMR spectrum in D_2O of a non-cross-linked block copolymer (**Figure S19**) clearly shows full disappearance of the acetyl peaks. It can be argued that we elaborate on a complex multi-step assembly procedure. However, it is important to note that from polymer synthesis and purification onwards, all step steps sequentially occur in a one-pot setting, only yielding low molecular weight by-products that are easily removed during the final dialysis step. All samples could be readily redispersed in phosphate buffered saline (PBS; pH 7.4). DLS (**Figure 3B**) indicated barely any alteration between the measured particle size before and after cross-linking with no significant influence of the type of cross-linker that was used in the reaction. To test whether the nanogels cross-linked with the ketal-containing 2, 2'-bis(aminoethoxy)propane can degrade in response to acidic pH, we monitored particle size and light scattering intensity as function of time by DLS. As shown in **Figure 3C-D**, exemplified for Man_1-based nanogels, cross-linking with 2, 2'-bis(aminoethoxy)propane (i.e. Man_1^{D}) renders the nanogels readily degradable into soluble unimers (cfr. size distribution graphs in **Figure 3D**) in response to acidic pH, whereas they remained stable for at least 48 h (longer time points not shown) at the physiological pH of 7.4. Nanogels cross-linked with 2, 2'-(ethylenedioxy)bis(ethylamine) (i.e. Man_1^{ND}) remained stable over time irrespective of pH, illustrating the crucial role of the cross-linking chemistry.

Subsequently, we investigated the functionality that was engineered into the nanogels. Firstly, to test whether the mannose repeating units exhibit selective lectin-binding activity we mixed mannosylated nanogels (Man_1^{D}) with Concanavalin A (ConA) and monitored nanogel agglutination by DLS. As a control, an identical experimental setup was used to test the galactosylated nanogels.

ConA is a lectin that has four binding sites at physiological pH and can interact with mannosyl and glucosyl moieties,[8] but not with galactosyl moieties. The immediate increase in size and light scattering intensity upon addition of ConA to mannosylated nanogels (**Figure 3E**), without change when ConA is added to galactosylated nanogels (Gal_1^{ND})(**Figure 3F**), clearly demonstrates the specific lectin-binding properties of the mannosylated nanogels (Supporting Information **Figure S21** provides further visual proof of specific lectin binding).

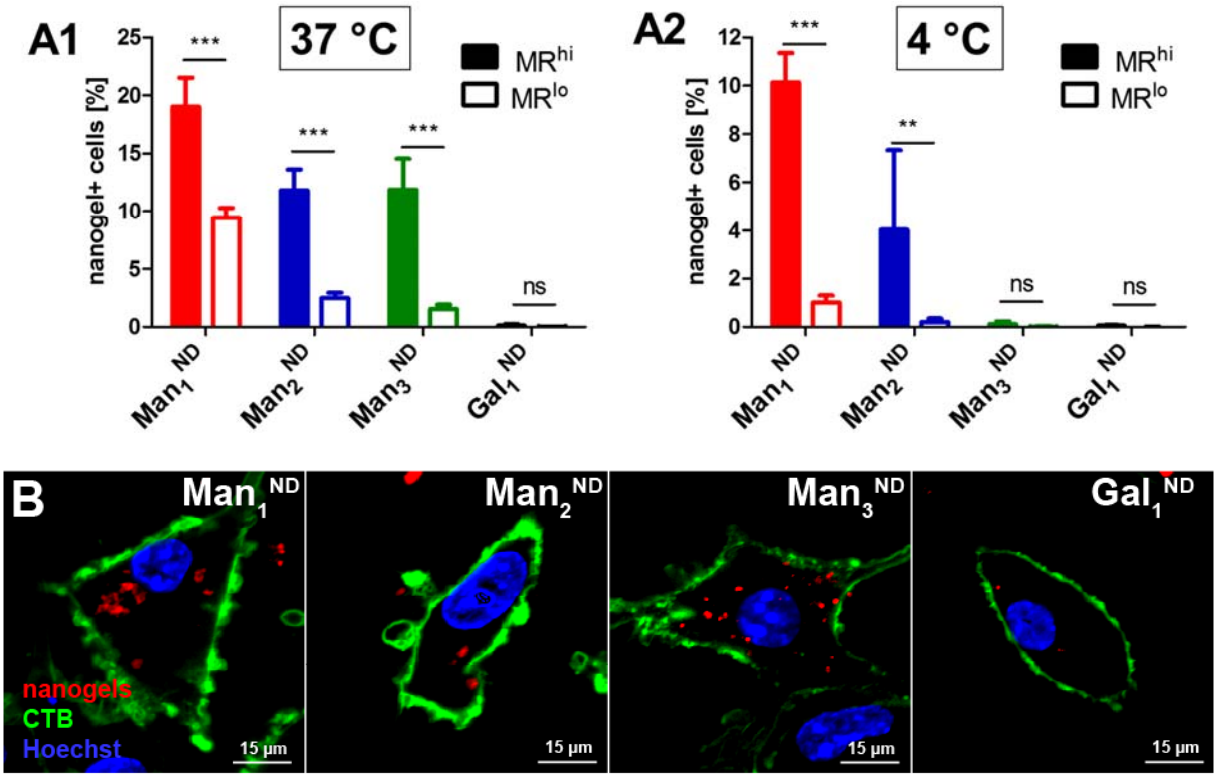

Figure 4. (A) Flow cytometry analysis of nanogels-bmDC association at 37 °C (A1) and at 4 °C (A2), discriminating between cell subsets that show high, respectively low expression of the mannose receptor. (n=3; $p<0.001$:***; $p<0.01$:**; $p>0.05$:ns). (B) Confocal images of DCs incubated with nanogels (red fluorescence) at 37 °C. Cell membrane was stained with AlexaFluor488 conjugated cholera toxin B (CTB) and cell nuclei were stained with Hoechst.

The sample codes (Man_1^{ND}), (Man_2^{ND}), (Man_3^{ND}) and (Gal_1^{ND}) correspond to the different polymer compositions listed in **Table 1**.

Secondly, as our final aim in the present work, we aimed at investigating the potential of the mannosylated nanogels for specific targeting of dendritic cells (DCs) that are known to express the mannose receptor. For this purpose we differentiated primary DCs from bone marrow isolated from the femurs and tibias of mice (bmDCs). Next we pulsed the bmDCs for 1h at respectively 37 °C or 4 °C to asses respectively dendritic cell uptake or cellular association of the nanogels, followed by anti-MR antibody staining and FACS analysis. In these set of experiments, only non-degradable nanogels were utilized to rule out the influence of nanogel degradation. Furthermore, we also verified (**Figure S22**) whether all nanogel solutions had similar fluorescence payload in order to allow for reliable comparison. This revealed to be the case, with only the smallest nanogels (Man_3^{ND}) having slightly higher fluorescence. In addition, a bmDC control sample was stained with an antibody cocktail for CD11c (cell surface marker for bmDC selection), anti-MR CD206 (anti-Mannose receptor), MHCII and CD86 (both cell surface markers for DC maturation) to elucidate the percentage of mannose receptor expression by the bmDCs and correlation of the latter with maturation of the cells. This revealed, as shown in **Figure S23** in Supporting Information, that all MR^{hi} cells are DCs, as these are also $CD11c^{hi}$, whereas MR-expression was observed on both mature ($MHCII^{hi}$, $CD86^{hi}$) and immature ($MHCII^{lo}$, $CD86^{lo}$) DC subsets. For the subsequent FACS analysis of the nanogels , as depicted in **Figure 4A1**, we selected both MR^{hi} and MR^{lo} cells subsets and compared them for nanogel association (i.e. cell surface binding or uptake). It is clear that at 37 °C, the MR^{hi} cell subset associates more efficiently to mannosylated nanogels than the MR^{lo} cell subset. Interestingly, the galactosylated nanogels exhibit very low cellular association, regardless the expression of the MR. However, as the mannose receptor is an endocytotic receptor,

one could expect a lower endocytotic activity for the MR^{lo} cell subset and therefore, the reduced association of the mannosylated nanogels with the MR^{lo} relative to the MR^{hi} cell subset cannot be seen as conclusive proof for MR-specific binding.

Despite this, the observation that galactosylated nanogels do not show any cellular association already provides a clear indication of the role of the MR in cellular binding of the nanogels. Further, a more conclusive proof of MR-specific nanogel binding was obtained from the experiment performed at 4 °C that is shown in **Figure 4A2**. At 4 °C, active endocytosis is abolished and only cell surface receptor binding or non-specific binding can take place. Under these experimental conditions, significantly higher association of mannosylated nanogels to the MR^{hi} cell subset is observed for both Man_1^{ND} and Man_2^{ND} whereas no significant cell association to both cell subsets is observed for the smallest Man_3^{ND} nanogels. Galactosylated nanogels (Gal_1^{ND}) on their side did again not show any cell association under these conditions, thereby unambiguously demonstrating the receptor-specific binding of the mannosylated nanogels to MR^{hi} DCs. A second observation involves the extent of nanogel-MR^{hi} DC binding at 4 °C. This strongly depends on the size of the nanogels, where bigger nanogels bind more efficient than smaller ones. This could be attributed to the higher fluorescent payload of larger nanogels relative to smaller ones. However, the FACS histogram in **Figure S23** show a distinct population of nanogels+ cells appear, which could suggest a higher avidity of bigger nanogels compared to smaller ones as bigger nanogels will expose more ligand copies than smaller ones. In this regard it is also noteworthy to mention the effect of superselectivity that can occur in case of larger nanogels. This aspect of multivalency has recently been described by Frenkel and co-workers and could explain a faster than linear increase of cell-bound nanogels with the density of available mannose ligands.[59–61] Such trend appears in our present work but requires more in depth investigation.

In a final series of experiments, we used confocal microscopy to investigate whether the nanogels are internalized by the DCs or merely bound to the cell membrane. As shown in **Figure 4B**, depicting bmDCs that were pulsed during 1 h with nanogels at 37 °C, nanogels are clearly found inside cells, proving they are actively endocytosed.

CONCLUSIONS

To summarize, we reported in this paper on the design of fully hydrophilic glycosylated nanogels with tailorable dimensions below 100 nm, via self-assembly of amphiphilic, but fully hydrophobic, precursor block copolymers. The use of an activated ester based hydrophobic block permitted the introduction of (degradable) cross-links and covalent linkage of fluorophores. We demonstrated that mannosylated nanogels promoted ligand-receptor recognition to lectins in solution and on the cell surface of primary DCs. Under physiological conditions mannosylated nanogels are efficiently internalized by DCs. Given the multiple opportunities to introduce further functionalities, e.g. via reactive ester approach or end-group modification, we focus our current research endeavors to engineer the nanogel interior, respectively surface, with vaccine antigens and immune-stimulatory small molecules.

ASSOCIATED CONTENT

Supporting Information. The Supporting Information is available free of charge on the ACS Publications website and contains supplemental data (PDF).

AUTHOR INFORMATION

Corresponding Authors

Prof. Dr. Bruno De Geest, Department of Pharmaceutics, Ghent University, Ghent, Belgium. Br.degeest@ugent.be

Dr. Lutz Nuhn, Department of Pharmaceutics, Ghent University, Ghent, Belgium. Lutz.nuhn@ugent.be

Funding Sources

The authors declare no competing financial interests.

FWO-Flanders, Ghent University Special Research Fund Flemish, Foundation Against Cancer.

ACKNOWLEDGMENT

RDC and NV acknowledge the Special Research Fund of Ghent University for a PhD scholarship. BDG acknowledges the Flemish Foundation against Cancer, FWO Flanders and the Special Research Fund of Ghent University (BOF-GOA) for funding. Rudolf Zentel is acknowledged for providing access to the THF-SEC.

REFERENCES

(1) East, L. *Biochim. Biophys. Acta - Gen. Subj.* **2002**, *1572*, 364–386.

(2) Banchereau, J.; Steinman, R. M. *Nature* **1998**, *392*, 245–252.

(3) Tan, M. C.; Mommaas, A. M.; Drijfhout, J. W.; Jordens, R.; Onderwater, J. J.; Verwoerd, D.; Mulder, A. A.; van der Heiden, A. N.; Scheidegger, D.; Oomen, L. C.; Ottenhoff, T. H.; Tulp, A.; Neefjes, J. J.; Koning, F. *Eur. J. Immunol.* **1997**, *27*, 2426–2435.

(4) Movahedi, K.; Schoonooghe, S.; Laoui, D.; Houbracken, I.; Waelput, W.; Breckpot, K.; Bouwens, L.; Lahoutte, T.; De Baetselier, P.; Raes, G.; Devoogdt, N.; Van Ginderachter, J. A. *Cancer Res.* **2012**, *72*, 4165–4177.

(5) Geijtenbeek, T. B. .; Torensma, R.; van Vliet, S. J.; van Duijnhoven, G. C. .; Adema, G. J.; van Kooyk, Y.; Figdor, C. G. *Cell* **2000**, *100*, 575–585.

(6) Wang, S.-K.; Liang, P.-H.; Astronomo, R. D.; Hsu, T.-L.; Hsieh, S.-L.; Burton, D. R.; Wong, C.-H. *Proc. Natl. Acad. Sci. U. S. A.* **2008**, *105*, 3690–3695.

(7) Becer, C. R.; Gibson, M. I.; Geng, J.; Ilyas, R.; Wallis, R.; Mitchell, D. A.; Haddleton, D. M. *J. Am. Chem. Soc.* **2010**, *132*, 15130–15132.

(8) Mann, D. A.; Kanai, M.; Maly, D. J.; Kiessling, L. L. *J. Am. Chem. Soc.* **1998**, *120*, 10575–10582.

(9) Lundquist, J. J.; Toone, E. J. *Chem. Rev.* **2002**, *102*, 555–578.

(10) Mammen, M.; Choi, S.; Whitesides, G. *Angew. Chem. Int. Ed. Engl.* **1998**, *37*, 2755–2794.

(11) Fasting, C.; Schalley, C. A.; Weber, M.; Seitz, O.; Hecht, S.; Koksch, B.; Dernedde, J.; Graf, C.; Knapp, E.-W.; Haag, R. *Angew. Chem. Int. Ed. Engl.* **2012**, *51*, 10472–10498.

(12) Belardi, B.; Bertozzi, C. R. *Chem. Biol.* **2015**, *22*, 983–993.

(13) Becer, C. R. *Macromol. Rapid Commun.* **2012**, *33*, 742–752.

(14) Moon, J. J.; Huang, B.; Irvine, D. J. *Adv. Mater.* **2012**, *24*, 3724–3746.

(15) De Koker, S.; Lambrecht, B. N.; Willart, M. a; van Kooyk, Y.; Grooten, J.; Vervaet, C.; Remon, J. P.; De Geest, B. G. *Chem. Soc. Rev.* **2011**, *40*, 320–339.

(16) Hubbell, J. a; Thomas, S. N.; Swartz, M. a. *Nature* **2009**, *462*, 449–460.

(17) De Geest, B. G.; Willart, M. a.; Lambrecht, B. N.; Pollard, C.; Vervaet, C.; Remon, J. P.; Grooten, J.; De Koker, S. *Angew. Chem. Int. Ed. Engl.* **2012**, *51*, 3862–3866.

(18) De Geest, B. G.; Willart, M. A.; Hammad, H.; Lambrecht, B. N.; Pollard, C.; Bogaert, P.;

De Filette, M.; Saelens, X.; Vervaet, C.; Remon, J. P.; Grooten, J.; De Koker, S. *ACS Nano* **2012**, *6*, 2136–2149.

(19) Moon, J. J.; Suh, H.; Bershteyn, A.; Stephan, M. T.; Liu, H.; Huang, B.; Sohail, M.; Luo, S.; Ho Um, S.; Khant, H.; Goodwin, J. T.; Ramos, J.; Chiu, W.; Irvine, D. J. *Nat Mater* **2011**, *10*, 243–251.

(20) Kwon, Y. J.; James, E.; Shastri, N.; Fréchet, J. M. J. *Proc. Natl. Acad. Sci. U. S. A.* **2005**, *102*, 18264–18268.

(21) Nembrini, C.; Stano, A.; Dane, K. Y.; Ballester, M.; van der Vlies, A. J.; Marsland, B. J.; Swartz, M. A.; Hubbell, J. A. *Proc. Natl. Acad. Sci.* **2011**, *108*, E989–E997.

(22) Reddy, S. T.; van der Vlies, A. J.; Simeoni, E.; Angeli, V.; Randolph, G. J.; O'Neil, C. P.; Lee, L. K.; Swartz, M. A.; Hubbell, J. A. *Nat. Biotechnol.* **2007**, *25*, 1159–1164.

(23) Lynn, G. M.; Laga, R.; Darrah, P. A.; Ishizuka, A. S.; Balaci, A. J.; Dulcey, A. E.; Pechar, M.; Pola, R.; Gerner, M. Y.; Yamamoto, A.; Buechler, C. R.; Quinn, K. M.; Smelkinson, M. G.; Vanek, O.; Cawood, R.; Hills, T.; Vasalatiy, O.; Kastenmüller, K.; Francica, J. R.; Stutts, L.; Tom, J. K.; Ryu, K. A.; Esser-Kahn, A. P.; Etrych, T.; Fisher, K. D.; Seymour, L. W.; Seder, R. A. *Nat. Biotechnol.* **2015**, *33*, 1201–1210.

(24) Jewell, C. M.; Bustamante Lopez, S. C.; Irvine, D. J. *Proc. Natl. Acad. Sci.* **2011**, *108*, 15745–15750.

(25) Zhang, Q.; Su, L.; Collins, J.; Chen, G.; Wallis, R.; Mitchell, D. a.; Haddleton, D. M.; Becer, C. R. *J. Am. Chem. Soc.* **2014**, *136*, 4325–4332.

(26) Fishman, J. M.; Kiessling, L. L. *Angew. Chem. Int. Ed. Engl.* **2013**, *52*, 5061–5064.

(27) Geng, J.; Mantovani, G.; Tao, L.; Nicolas, J.; Chen, G.; Wallis, R.; Mitchell, D. A.; Johnson, B. R. G.; Evans, S. D.; Haddleton, D. M. **2007**, *19*, 15156–15163.

(28) Song, E.-H.; Manganiello, M. J.; Chow, Y.-H.; Ghosn, B.; Convertine, A. J.; Stayton, P. S.; Schnapp, L. M.; Ratner, D. M. *Biomaterials* **2012**, *33*, 6889–6897.

(29) Kang, B.; Okwieka, P.; Schöttler, S.; Winzen, S.; Langhanki, J.; Mohr, K.; Opatz, T.; Mailänder, V.; Landfester, K.; Wurm, F. R. *Angew. Chemie Int. Ed.* **2015**, *54*, 7436–7440.

(30) Cui, L.; Cohen, J. A.; Broaders, K. E.; Beaudette, T. T.; Fr, J. M. J. **2011**, 949–957.

(31) Canton, I.; Battaglia, G. *Chem. Soc. Rev.* **2012**, *41*, 2718–2739.

(32) Ferguson, C. J.; Hughes, R. J.; Nguyen, D.; Pham, B. T. T.; Gilbert, R. G.; Serelis, A. K.; Such, C. H.; Hawkett, B. S. *Macromolecules* **2005**, *38*, 2191–2204.

(33) Nuhn, L.; Hirsch, M.; Krieg, B.; Koynov, K.; Fischer, K.; Schmidt, M.; Helm, M.; Zentel, R. *ACS Nano* **2012**, *6*, 2198–2214.

(34) Ambrosi, M.; Batsanov, A.; Cameron, N.; Davis, B.; Howard, J.; Hunter, R. *J. Chem. Soc. Perkin Trans. 1* **2002**, 45–52

(35) Randolph, G. J.; Angeli, V.; Swartz, M. A. *Nat Rev Immunol* **2005**, 617–628.

(36) Shen, Z.; Reznikoff, G.; Dranoff, G.; Rock, K. L. *J. Immunol.* **1997**, *158*, 2723–2730.

(37) Heath, W. R.; Belz, G. T.; Behrens, G. M. N.; Smith, C. M.; Forehan, S. P.; Parish, I. A.; Davey, G. M.; Wilson, N. S.; Carbone, F. R.; Villadangos, J. A. *Immunol. Rev.* **2004**, *199*, 9–26.

(38) Wollenberg, A.; Mommaas, M.; Oppel, T.; Schottdorf, E. M.; Gunther, S.; Moderer, M. *J Invest Dermatol* **2002**, *118*, 327–334.

(39) Zehner, M.; Chasan, A. I.; Schuette, V.; Embgenbroich, M.; Quast, T.; Kolanus, W.; Burgdorf, S. *Proc. Natl. Acad. Sci. U. S. A.* **2011**, *108*, 9933–9938.

(40) Eberhardt, M.; Mruk, R.; Zentel, R.; Theato, P. *Eur. Polym. J.* **2005**, *41* (7), 1569–1575.

(41) Boyer, C.; Davis, T. P. *Chem. Commun.* **2009**, 6029–6031.

(42) Li, Y.; Duong, H. T. T.; Jones, M. W.; Basuki, J. S.; Hu, J.; Boyer, C.; Davis, T. P. *ACS Macro Lett.* **2013**, *2*, 912–917.

(43) Das, A.; Theato, P. *Chem. Rev.* **2016**, *116*, 1434–1495.

(44) Dong, C.-M.; Sun, X.-L.; Faucher, K. M.; Apkarian, R. P.; Chaikof, E. L. *Biomacromolecules* **2004**, *5*, 224–231.

(45) Spaltenstein, A.; Whitesides, G. M. *J. Am. Chem. Soc.* **1991**, *113*, 686–687.

(46) Yu, K.; Kizhakkedathu, J. N. *Biomacromolecules* **2010**, *11*, 3073–3085.

(47) Boyer, C.; Bulmus, V.; Davis, T. P.; Ladmiral, V.; Liu, J.; Perrier, S. *Chem. Rev.* **2009**, *109*, 5402–5436.

(48) Graisuwan, W.; Zhao, H.; Kiatkamjornwong, S.; Theato, P.; Hoven, V. P. *J. Polym. Sci. Part A Polym. Chem.* **2015**, *53*, 1103–1113.

(49) Nuhn, L.; Tomcin, S.; Miyata, K.; Mailänder, V.; Landfester, K.; Kataoka, K.; Zentel, R. *Biomacromolecules* **2014**, *15*, 4111–4121.

(50) O'Reilly, R. K.; Hawker, C. J.; Wooley, K. L. *Chem. Soc. Rev.* **2006**, *35*, 1068–1083.

(51) Binauld, S.; Stenzel, M. H. *Chem. Commun.* **2013**, *49*, 2082–2102.

(52) Duong, H. T. T.; Marquis, C. P.; Whittaker, M.; Davis, T. P.; Boyer, C. *Macromolecules*

2011, *44*, 8008–8019.

(53) Jain, R.; Standley, S. M.; Fréchet, J. M. J. *Macromolecules* **2007**, *40*, 452–457.

(54) Grover, G. N.; Alconcel, S. N. S.; Matsumoto, N. M.; Maynard, H. D. *Macromolecules* **2009**, *42*, 7657–7663.

(55) Roth, P. J.; Boyer, C.; Lowe, A. B.; Davis, T. P. *Macromol. Rapid Commun.* **2011**, *32*, 1123–1143.

(56) Boyer, C.; Bulmus, V.; Davis, T. P. *Macromol. Rapid Commun.* **2009**, *30*, 493–497.

(57) Willcock, H.; O'Reilly, R. K. *Polym. Chem.* **2010**, *1*, 149–157.

(58) Zhang, Q.; Voorhaar, L.; De Geest, B. G.; Hoogenboom, R. *Macromol. Rapid Commun.* **2015**, *36*, 1177–1183.

(59) Dubacheva, G. V.; Curk, T.; Mognetti, B. M.; Auzély-Velty, R.; Frenkel, D.; Richter, R. P. *J. Am. Chem. Soc.* **2014**, *136*, 1722–1725.

(60) Martinez-Veracoechea, F. J.; Frenkel, D. *Proc. Natl. Acad. Sci. U. S. A.* **2011**, *108*, 10963–10968.

(61) Dubacheva, G. V; Curk, T.; Auzély-Velty, R.; Frenkel, D.; Richter, R. P. *Proc. Natl. Acad. Sci. U. S. A.* **2015**, *112*, 5579–5584.